J. Fluid Mech. (1990), *vol.* 213, *pp.* 611–639
Printed in Great Britain

Self-excited oscillations and mixing in a heated round jet

By PETER A. MONKEWITZ[1], DIETRICH W. BECHERT[2], BERND BARSIKOW[2] AND BERNHARD LEHMANN[2]

[1] Department of Mechanical, Aerospace and Nuclear Engineering, University of California, Los Angeles, CA 90024-1597, USA

[2] DLR, Institut fuer Turbulenzforschung, Mueller-Breslau-Strasse 8, 1000 Berlin 12, West Germany

An axisymmetric hot-air jet discharging into cold ambient air is investigated experimentally. We consider the transitional regime, that is, Reynolds numbers at which the jet is initially laminar. In the first part of the paper it is demonstrated by several different experiments that, for sufficiently low Reynolds number and a ratio of jet exit to ambient density below approximately 0.7, global oscillations of the 'jet column' become self-excited, a behaviour which is related to local absolute instability in the potential core region. The onset of the global oscillations is identified as a Hopf bifurcation and two axisymmetric global modes are observed below the critical density ratio. Finally, it is shown that in the (self-excited) limit-cycle regime the spreading of the hot jet is intermittently quite spectacular, with half-angles in excess of 45°. Using flow visualization, this large spreading of low-density jets is related to the generation of strong 'side jets' emanating from the jet column.

1. Introduction

The interest in jets of non-uniform density and composition, with and without chemical reaction (combustion), has been stimulated in the last century by the observation of 'singing flames' and the extreme sensitivity of various inhomogeneous jets to sound. A delightful account of such experiments, which include the dramatic increase of jet spreading by musical forcing, the creation of a bifurcating hot jet/plume by sound as well as the reading of poetry to flames, can be found in the sixth lecture of Tyndall (1867) delivered at the Royal Institution in London.

More recently, problems related to jet engine exhausts and to combustion have led to a renewed interest in the behaviour of inhomogeneous (hot) jets. The present experiments in particular are focused on jets which are inertia dominated, i.e. where buoyancy effects are minimal near the nozzle. To quickly fix ideas, the operating conditions we consider here are specified in table 1 in terms of the most important non-dimensional parameters. Besides the definition and range of parameters, the table also contains, for convenience, a list of reference quantities. The subscripts ∞ and j refer to ambient conditions outside the jet and to conditions at the centre of the nozzle exit-plane, respectively. Two features of the table call for comments. First, the equation of state for an ideal gas at constant pressure, satisfied with good accuracy in our hot air jet, has been used to eliminate reference temperatures throughout. Second, special attention is drawn to the fact that the kinematic viscosity ν, used in the Reynolds number, is evaluated at the average $\frac{1}{2}(T_j+T_\infty)$ between jet and ambient temperature, which is approximately the mean temperature at the centre of the jet shear layer where viscous effects may be relevant.

Reference quantities:	D	jet nozzle diameter
	U_j	jet exit velocity
	ρ_∞	ambient density
	ν_{ref}	kinematic viscosity at $\frac{1}{2}(T_j+T_\infty)$
	k_{ref}	thermal conductivity at $\frac{1}{2}(T_j+T_\infty)$

Non-dimensional parameter		Range in the present experiments
Primary parameters		
Density ratio	$S=\rho_j/\rho_\infty$	0.45–1
Reynolds number	$Re=U_jD/\nu_{ref}$	5×10^3–5×10^4
Mach number	$M=U_j/a_\infty$	0.025–0.3
		Not varied independently of Re
Boundary conditions at the nozzle exit (velocity and density profiles)		
Parameters not systematically varied		
Richardson number	$Ri=gD(1-S)/(SU_j^2)$	$<2\times10^{-3}\ll1$
		Effects of buoyancy negligible near nozzle
Prandtl number	$Pr=\nu_{ref}/k_{ref}$	≈0.7 (constant)
Ratio of specific heats	$\gamma=c_p/c_v$	≈1.4 (constant)
Eckert number (for ideal gas)	$Ec=M^2S(\gamma-1)/(1-S)$	$<0.04\ll Re$
		Negligible heat generation by viscous effects

TABLE 1. Summary of the most important non-dimensional parameters pertinent to the present experiments and their ranges.

Among early studies in the parameter range of table 1, the work by Corrsin & Uberoi (1947) provided one of the first comprehensive surveys of mean and turbulence quantities in a hot air jet. Extensive data on high-subsonic and supersonic heated jets, including the effect of acoustic forcing, have been compiled by Lepicovski *et al.* (1988). On the theoretical side, Michalke (1971, 1984) studied the linear stability of heated gas jets on a locally parallel basis and discovered additional instability modes at a ratio $S_{loc}=\rho_c/\rho_\infty$ of local centreline and ambient density equal to 0.5, which were later related to absolute instability by Monkewitz & Sohn (1986, 1988). A brief summary of the stability results, together with an introduction to the concept of absolute instability and its connection to (linear) global instability, i.e. self-excitation, is given in §2.

The discovery of local absolute instability in the potential-core region of low-density jets, exhausting into higher density fluid, strongly suggested the possibility of self-excited jet oscillations. However, because the jet develops spatially, self-excitation does not follow automatically from the absolute instability of local velocity and density profiles, as discussed in detail by Huerre & Monkewitz (1990). The question of whether, and under what conditions, self-excited oscillations occur in low-density jets therefore requires further investigation, and has been the primary motivation for this heated-jet study, previously summarized by Monkewitz & Bechert (1988) and Monkewitz *et al.* (1988), as well as for the helium/nitrogen jet experiments of Sreenivasan, Raghu & Kyle (1989) and Kyle (1988). Related work in a dump combustor configuration has been carried out by Subbarao (1987).

After describing the experimental facility in §3, we show in §4, the first of the two

central sections, that self-excited oscillations are indeed observed in the heated jet for jet-exit densities below approximately 70% of the ambient density, which corresponds closely to the boundary of local absolute instability. A further main requirement for a clean self-excited response is found experimentally to be a laminar initial jet shear layer, i.e. a moderately low Reynolds number and an extremely quiet facility. To ascertain the self-excited nature of the jet flow itself, other sources of self-excitation, such as coupling of the flow to acoustic facility resonances, are first ruled out. Then, several independent tests of self-excitation are applied. They include near-field pressure measurements to identify the Hopf bifurcation (see e.g. Joseph 1976, Chapter II) to self-excited global oscillations, an acoustic forcing experiment to demonstrate insensitivity to low-level forcing in the self-excited regime, and finally a transient experiment.

The second main topic of the paper, to which §5 is devoted, is the spectacular jet spreading associated with self-excitation, which was discovered by flow visualization, using Schlieren as well as light scattering from seeding particles. After characterizing the mean flow, we demonstrate in particular that the large spreading is not axisymmetric and that it can be related to the formation of strong 'side jets'. Finally, a comparison with highly forced cold jets leads us to speculate on the mechanism of their generation. Other flows with spreading characteristics and azimuthal structures (side jets) very similar to our heated jet have recently been found by Lehmann *et al.* (1988). They are hydrogen and methane jet diffusion flames, for which the density ratios are $S = 0.07$ and $S = 0.55$, respectively. On the other hand, heated air jets at higher Reynolds and Mach numbers appear to spread essentially like cold jets (Lepicovski *et al.* 1988), and do not exhibit the pronounced side jets found at low speed.

2. Local absolute instability and global oscillations

In the following, we give a brief introduction to the topic of local and global hydrodynamic instability as related to the low-density axisymmetric jet discharging into denser ambient fluid.

The linear stability analysis of local jet profiles by Monkewitz & Sohn (1986, 1988) revealed that the nature of the instability can change from (locally) convective to absolute as the ratio $S_{\mathrm{loc}} = \rho_c/\rho_\infty$ of local centreline to ambient density is lowered. Very briefly, the terms convective and absolute characterize the linear impulse response of an unstable parallel base flow in a frame of reference which is fixed to the nozzle for the jet under consideration. A flow is referred to as absolutely unstable if, after an initial impulsive 'push', the disturbance energy grows in time at any fixed spatial location. If, on the other hand, disturbance energy is ultimately convected away faster than it is produced, one speaks of convective instability. As a consequence, any steady-periodic disturbances observed in a convectively unstable flow are the result of continuous external forcing by, for instance, free-stream disturbances. For a thorough discussion of these concepts the reader is referred to Bers (1983) and Huerre & Monkewitz (1985, 1990).

To study the linear stability of the heated jet, Monkewitz & Sohn (1986, 1988) used a family of model profiles for the mean velocity and density, assumed the fluid to be an inviscid ideal gas ($Re = \infty, Pr \neq 0$), and neglected buoyancy effects as well as heat generation by friction ($Ri = 0$, $Ec/Re = 0$). Surveying the effect of the remaining parameters such as Mach number and profile shape, they found the highest density ratio for absolute instability to be $S_{\mathrm{loc}} = 0.72$. This value was obtained for zero Mach

number and for axisymmetric disturbances on a profile with a vorticity thickness δ_ω ($\delta_\omega = U_j/|\mathrm{d}U/\mathrm{d}r|_{max}$) of 8.4% of the local jet diameter (measured to the half-velocity point). Furthermore, the frequency of locally dominant modes was found to scale as a Strouhal number based on the jet diameter with values between 0.25 and 0.5 (figure 6*b* of Monkewitz & Sohn 1988).

The question of how these local flow properties, i.e. convective and absolute instability, are related to the observed global behaviour of the actual non-parallel flow system has been discussed by Fuchs, Ko & Bers (1981) and more fully by Chomaz, Huerre & Redekopp (1988), Monkewitz (1988) and Huerre & Monkewitz (1990). Analogous to convective and absolute instability in parallel systems, a distinction between 'amplifier' and 'oscillator' behaviour is made in non-parallel systems.

If the flow is nowhere absolutely unstable, i.e. convectively unstable or stable everywhere, all local modes and consequently all global modes are time-damped, provided the system contains no additional global pressure feedback (e.g. from a downstream edge) or active control loop. Therefore such a flow behaves as an 'amplifier' that spatially amplifies selected external disturbances and ultimately returns to the undisturbed base state if all external excitation is turned off. In this context the terms local and global mode are used as follows. A local mode is obtained by an ordinary parallel stability analysis of a local mean profile, for which time and downstream distance x are separated out in a factor $\exp[ikx - i\omega t]$, with k and ω being the wavenumber and frequency, respectively. In contrast, a linear global mode is understood to be a solution of the unforced equations of motion, linearized around a non-parallel base flow, of the form $\boldsymbol{F}(x, y, z)\exp[-i\omega t]$, where the vector $\boldsymbol{F}$ contains all dependent variables.

On the other hand, if a system, starting from the undisturbed state, only needs a small 'push' to develop time-growing oscillations, it is self-excited and termed an 'oscillator'. As suggested by Chomaz *et al.* (1988), in the absence of global pressure feedback, such behaviour is only possible if the flow contains a region of absolute instability with a sufficient streamwise extent. Following the initial exponential growth of the disturbance, the system in many cases settles into a limit cycle. This final nonlinear state generally represents a global response which is *intrinsic* to the system and frequently independent of the nature of the initial impulse or even the nature of any additional, continuous, low-level forcing. Loosely stated, self-excitation of a system generally results in the largest possible amplitude of its 'preferred' mode, often associated with optimal momentum, heat and mass transport, in our case across the jet shear layer. The term 'preferred' mode is thereby not accidental but reflects the connection to the 'preferred' or 'jet column' mode in the homogeneous jet, established by Monkewitz, Huerre & Chomaz (1987). As we shall demonstrate, the hot jet falls into this 'oscillator' category below a critical overall density ratio $S_{crit} = \rho_j/\rho_\infty$ (based on the jet exit density ρ_j) that is close to the density ratio $S_{loc} = 0.72$ at which local absolute instability first occurs.

3. The experimental apparatus

The experimental facility, shown in figure 1, consisted of a compressed-air storage tank, a pressure reduction valve, a muffler, a 10 kW electric heater, a settling chamber with perforated plates, steel wool pack and turbulence screens and a final 100:1 contraction with a nozzle of $D = 15$ mm diameter, pointing vertically up. The entire aluminium nozzle block was kept at the same temperature as the jet air by a

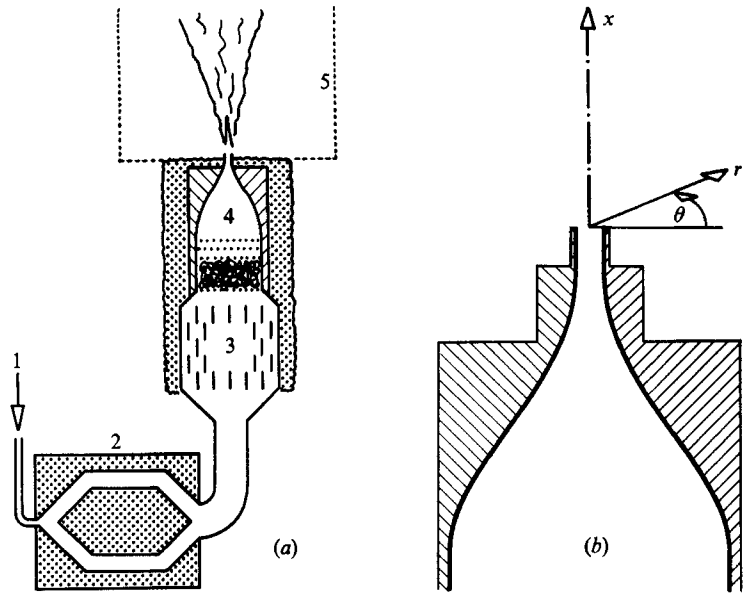

FIGURE 1. (*a*) Schematic of the heated jet facility (components not to scale): 1, compressed air supply; 2, muffler; 3, heater; 4, settling chamber and heated nozzle; 5, window screen. (*b*) Nozzle contraction, drawn to scale, with definition of the cylindrical coordinates.

second electric heater, in order to avoid cold boundary layers in the nozzle. The hot air was collected 235 cm above the nozzle and forced out of the room by a variable-speed fan.

Great care was taken to quiet the facility and to eliminate unsteady separation in all of its components. External sources of disturbances were also reduced to a minimum by first shrouding the jet from draughts in the laboratory which constitute very low-frequency disturbances. For this, a window screen, extending 35 cm beyond the jet nozzle, was placed around the jet at a radius of 25 cm. Then, the level of acoustic noise in the laboratory was minimized by carrying out the experiments at night with no traffic in or around the building, by switching off the exhaust fan during data acquisition, and by moving all electronic equipment with cooling fans into an adjacent room. The resulting r.m.s. turbulence level in the nozzle exit plane of the unheated jet was determined with a constant-temperature hot wire and found to be less than 0.05% for jet velocities of 10 and 30 m/s.

For the experiments the facility was instrumented as follows. The operating parameters were obtained from a platinum resistance thermometer in the settling chamber and from the settling chamber pressure. Throughout the study the near-field pressure at various locations outside the jet was monitored by a $\frac{1}{4}$ in. B&K microphone fitted with a standard nose cone to shield it from the entrainment flow. For some experiments, mainly in the cold jet, flow velocity was measured by hot wire, using a model DFVLR HDA III anemometer. Processing of the unsteady signals was performed on a Hewlett Packard 3562 Dynamic Signal Analyzer. To obtain mean data, on the other hand, a NiCr–Ni thermocouple probe with a junction of 0.2 mm diameter was used together with a total head probe of dimension 0.3×2 mm, connected to a micromanometer (system Rechenberg) or a Statham membrane pressure transducer. Flow visualization, finally, was carried out by two methods. The first was by Schlieren with a system based on two $f/10$ spherical mirrors

of 30 cm diameter. As light source a spark gap, DRELLO model BAL 1510, was used that discharged 10 J in a 500 ns pulse. All the photographs were taken with a slit of typically 0.4 mm and the knife edge oriented parallel to the jet axis. The second method of flow visualization used the scattering of laser light from passive seeding particles which consisted of either silicon carbide or tobacco smoke. Both types of particles were of approximately 1 μm and less in diameter and were injected into the jet fluid upstream of the heater in order to obtain a uniform distribution. A 4W Ar-Ion laser with a mechanical shutter was used as a stroboscopic light source. Its beam was expanded by cylindrical lenses into light sheets of 0.5–1 mm thickness that could be oriented either in an (x, r)-plane to provide a side view of the jet or in (r, θ)-planes for cross-sections, where (x, r, θ) are cylindrical coordinates defined in figure 1.

The experiments have been carried out with jet temperatures ranging from ambient, which was always close to 20 °C, to 400 °C. The Reynolds number, defined in table 1, ranged from 5000 to 50000 with the majority of the data taken at values of 7500 and 10000. $Re = 7500$ corresponds to an exit velocity of 7.5 m/s at a jet temperature of 20 °C ($S = 1$) and 16.4 m/s at 350 °C ($S = \rho_j/\rho_\infty = 0.47$). In the cold case the initial jet shear layer was found to be still laminar at a Reynolds number of 50000 and its vorticity thickness was determined by hot-wire anemometry as $\delta_\omega/D = 4.9Re^{-\frac{1}{2}}$, which amounts to 0.85 mm at $Re = 7500$. At the same Reynolds number and $S = 0.47$ the Richardson number (see table 1) is 6.2×10^{-4}, small enough for buoyancy effects to be insignificant in the potential-core region and beyond, except possibly in the low-speed peripheral region of the jet.

4. Experimental evidence of self-excited oscillations

4.1. *Flow visualization and near-field pressure spectra*

The most striking difference between cold jets and self-excited hot jets is the extraordinary spreading of the latter. It is illustrated by figure 2, which shows one schlieren image of a slightly heated jet for reference (jet temperature of 50 °C) and three snapshots of the hot jet at 200 °C, taken over a period of about 30 min under nominally identical conditions (see also Monkewitz & Bechert 1988). It is immediately noted that the spreading of density disturbances in figures 2(*b*)–2(*d*) is qualitatively different than in the slightly heated case 2(*a*): in what we shall show to be the self-excited regime, the visual spreading angle is most of the time dramatically larger than the usual angle of approximately 20° for the homogeneous case, but appears to vary considerably over time, an aspect that will be discussed in §5.

The corresponding near-field pressure spectra are shown on figure 3. The microphone is located outside the flow and is visible to the left of the nozzle on figure 2. Both the spectrum corresponding to the slightly heated jet (50 °C) of figure 2(*a*) and two spectra, taken 30 min apart, which correspond to the hot jet (200 °C) of figures 2(*b*)–2(*d*) are displayed. The latter spectra, which demonstrate good repeatability, are reminiscent of cylinder wake spectra and strongly suggest a limit cycle, i.e. a self-excited oscillation. In order to relate this behaviour to local absolute instability, other mechanisms leading to self-excited oscillations have to be eliminated. As no probes were inserted into the flow, any edge-tone-like probe interference (Hussain & Zaman 1978) is readily dismissed. It remains to be shown that neither collar tones nor acoustic cavity resonances are responsible for the observed oscillations.

Collar tones, which can occur in the presence of local separation at the end of the

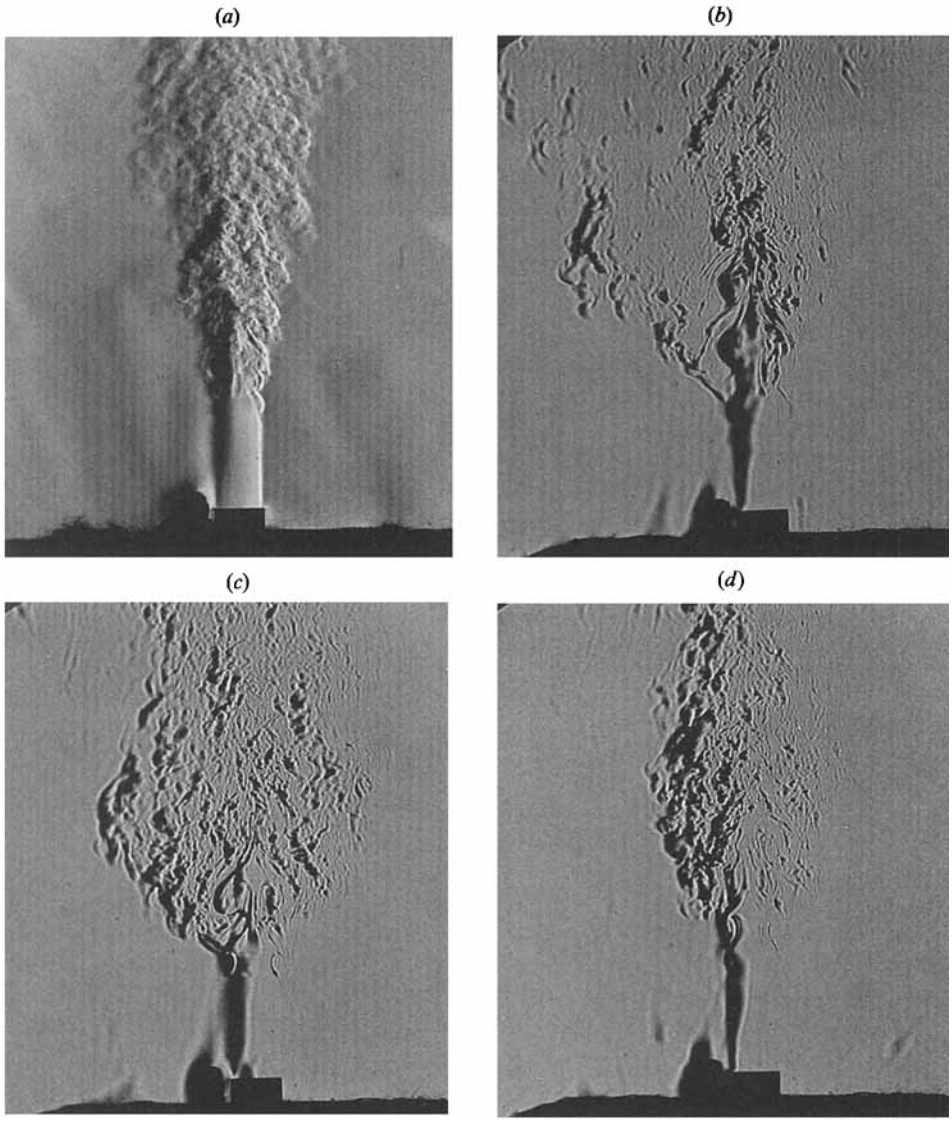

FIGURE 2. Spark schlieren views of the heated jet (0.5 μs exposure time). (*a*) Slightly heated jet with $S = \rho_j/\rho_\infty = 0.91$ ($T_j = 50$ °C) and $Re = 10^4$. (*b*), (*c*) and (*d*) Three views of the same self-excited jet at $S = 0.62$ ($T_j = 200$ °C) and $Re = 7500$.

contraction, have been eliminated as a possible explanation by the following experiment. The nozzle, which had a permanent straight tail section 2 diameters long, was extended with straight pipes of length $L_c = 1$, 2, and 3 diameters and the dominant frequency at constant jet velocity was measured in each case. According to Hussain & Hasan (1983, equation 1), the frequency of collar-tone modes decreases with L_c, and, in our case, would be approximately inversely proportional to L_c. This clearly does not correspond to our observations, shown on figure 4, of a global-mode frequency with only a weak dependence on the nozzle extension length L_c, probably related to the variation of initial jet shear-layer thickness.

Finally, the possibility of acoustic cavity (settling chamber, etc.) resonance, which would yield approximately constant frequencies at constant temperature, is ruled

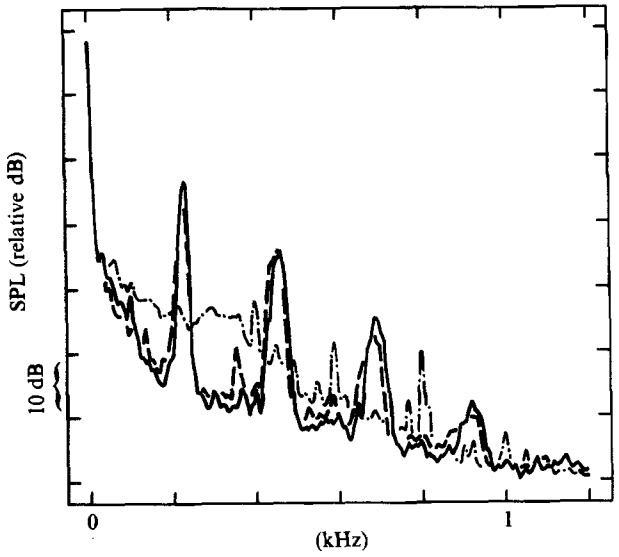

FIGURE 3. Near-field pressure spectra at $x/D = 0.2$ and $r/D = 1$ corresponding to the schlieren images of figure 2. Average of 100 spectra with bandwidth of 3.75 Hz. —·—·—·—, spectrum corresponding to figure 2(*a*); ——, ------, two spectra, taken 30 min apart, corresponding to figures 2(*b*)–2(*d*).

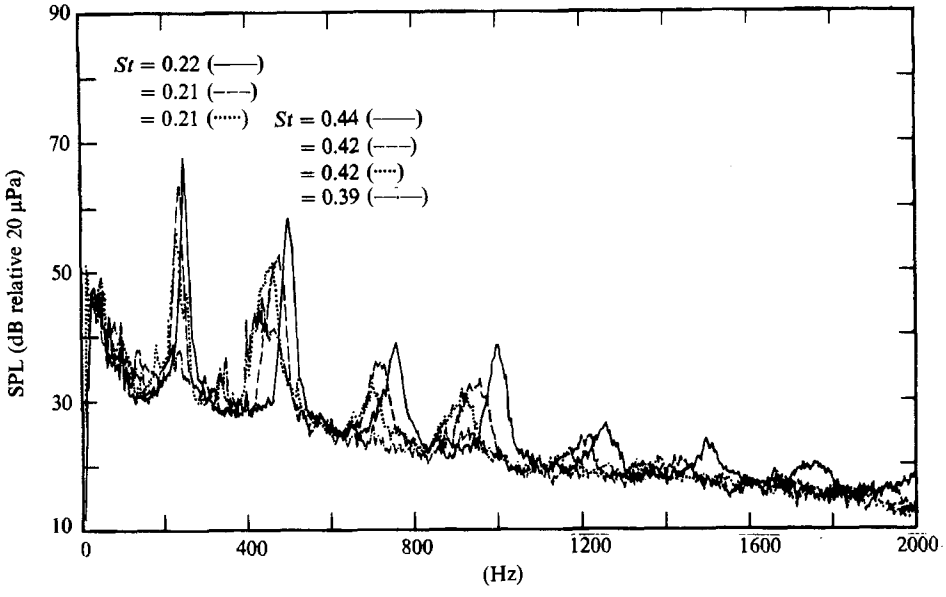

FIGURE 4. Near-field pressure spectra (3.75 Hz bandwidth) at $x/D = 0.2$ and $r/D = 1$ for $S = \rho_j/\rho_\infty = 0.47$, $Re = 7500$, and four different nozzle lengths: ——, standard nozzle; – – –, straight nozzle extension $L_c = 1D$; ·····, $L_c = 2D$; —·—·—, $L_c = 3D$. The Strouhal numbers $St = fD/U_j$ of the first two spectral peaks are indicated on the figure.

out on the basis of the Strouhal scaling observed on figure 5 (see also figure 3 of Monkewitz *et al.* 1988) and on figure 6. On this latter figure, the Strouhal numbers dominating the near-field pressure spectrum close to the nozzle are plotted for all cases during the present experiments in which line-dominated spectra were observed.

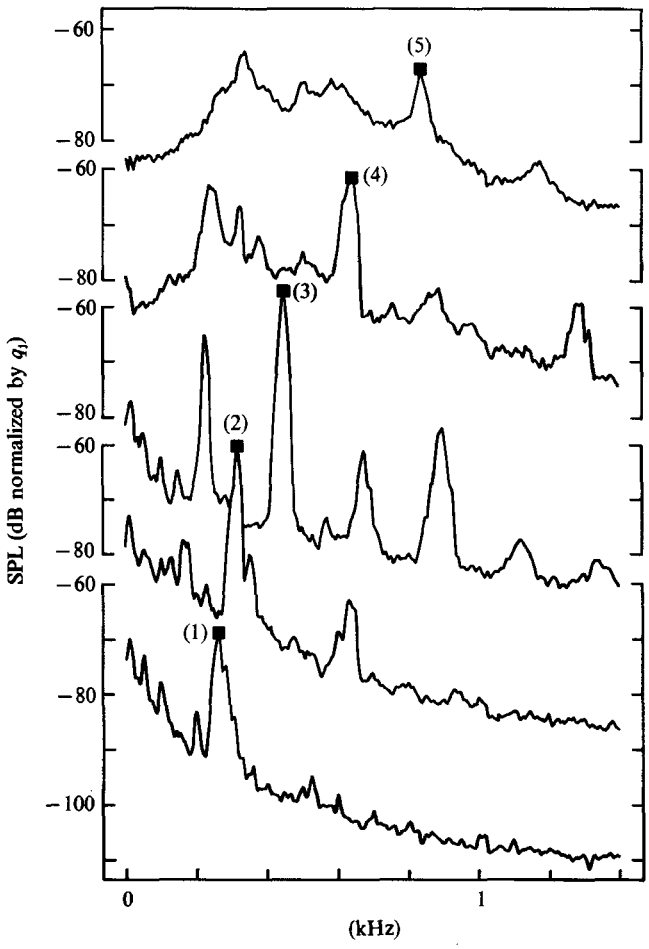

FIGURE 5. Near-field pressure spectra (3.75 Hz bandwidth, averaged over 75 realizations), normalized by the jet dynamic head $q_j = \frac{1}{2}\rho_j U_j^2$, at $x/D = 0.67$ and $r/D = 1.3$ for $S = \rho_j/\rho_\infty = 0.51$ and different jet velocities. The amplitudes and Strouhal numbers below refer to the main peaks indicated by ■. (1), $Re = 4900$ ($U_j = 9.83$ m/s), peak at $St \equiv fD/U_j = 0.40$ and -69 dB; (2), $Re = 5700$ ($U_j = 11.4$ m/s), peak at $St = 0.42$ and -60 dB; (3), $Re = 7400$ ($U_j = 14.8$ m/s), peak at $St = 0.45$ and -57 dB; (4), $Re = 10000$ ($U_j = 20.0$ m/s), peak at $St = 0.48$ and -62 dB; (5), $Re = 12400$ ($U_j = 24.7$ m/s), peak at $St = 0.51$ and -67 dB.

Owing to the lack of an obvious control parameter, the dimensional jet velocity has been chosen as abscissa. The peak Strouhal numbers are all found to be in the range of 0.25 to 0.5 and correspond to axisymmetric large-scale structures (vortex rings) in flow visualizations. It is noted in passing that, in support of the previous result for variable L_c, the dominant Strouhal numbers are seen to decrease slightly with increasing initial shear layer thickness, i.e. decreasing jet velocity. Both the range of Strouhal numbers and the axisymmetry are completely consistent with the analysis of Monkewitz & Sohn (1986, 1988), which suggests that non-axisymmetric global modes can only become self-excited below a density ratio of about 0.3. Thus the notion is supported that the observed strong oscillations are related to local absolute instability, i.e. to the effect of upstream-moving *vortical* instability waves (Huerre & Monkewitz 1990), and not to some other resonance mechanism.

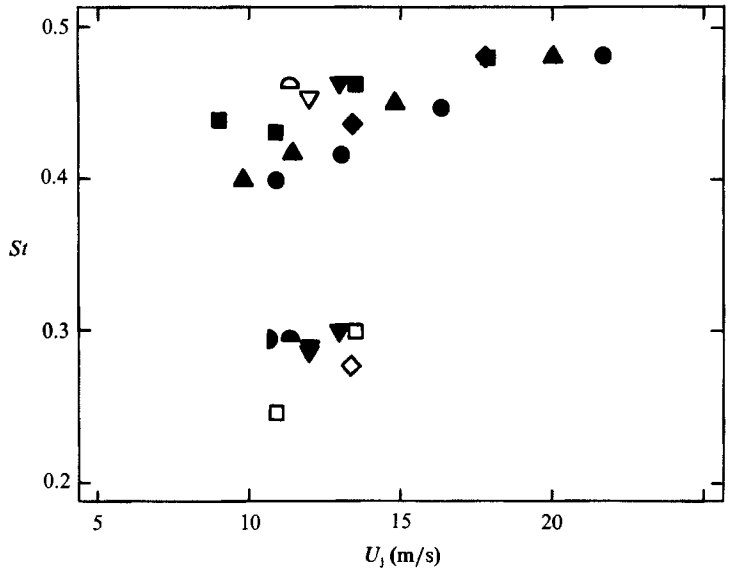

FIGURE 6. Dominant Strouhal numbers $St = fD/U_j$ versus jet velocity U_j for all cases in which the near-field pressure spectrum, measured at $x/D = 0.67$ and $r/D = 1.3$, shows strong peaks. ○, $S = \rho_j/\rho_\infty = 0.47$; △, 0.51; □, 0.55; ◇, 0.56; ▽, 0.62; ⌓, 0.65; ▷, 0.69. Solid and open symbols correspond to primary and unrelated (in frequency) secondary peaks, respectively.

4.2. *The parameter range for self-excited global oscillations and the character of the bifurcation*

The next task is to explore the parameter range of density ratio S, Reynolds number, initial shear layer thickness, and Mach number in which near-field pressure spectra are line-dominated. With a few exceptions we shall not consider hot-wire spectra, which are much easier to misinterpret since, even in the absence of self-excitation, they can be *locally* very peaky in a transitional jet, while the microphone, being sensitive to non-local jet oscillations, provides a better overall picture of the state of the flow field.

4.2.1. *The effect of density ratio*

First, the density ratio was varied at a constant Reynolds number of 7500. At lower values of the Reynolds number the signal to electronic noise ratio of the microphone started to deteriorate and, more importantly, the jet became more and more susceptible to external disturbances such as draughts and noise. The resulting pressure spectra near the nozzle are collected on figure 7. They show that distinct spectral lines develop below a density ratio $S = 0.69$ with the dominant lines between 30 and 40 dB above the noise. Note that at constant Reynolds number the jet velocity and, according to the Strouhal scaling, the dominant frequency increase with temperature.

Figure 7 also distinctly shows the existence of two axisymmetric global modes, which is fully consistent with the model analysis of Chomaz *et al.* (1988). It appears that, at the particular Reynolds number of 7500, a mode, designated Mode I, with a Strouhal number around $St \approx 0.3$ dominates for $0.69 \geqslant S \geqslant 0.62$, while for $0.55 \geqslant S \geqslant 0.47$ a Mode II takes over with a peak Strouhal number of $St \approx 0.45$ in the near-field pressure spectrum near the nozzle. This latter mode is characterized by the

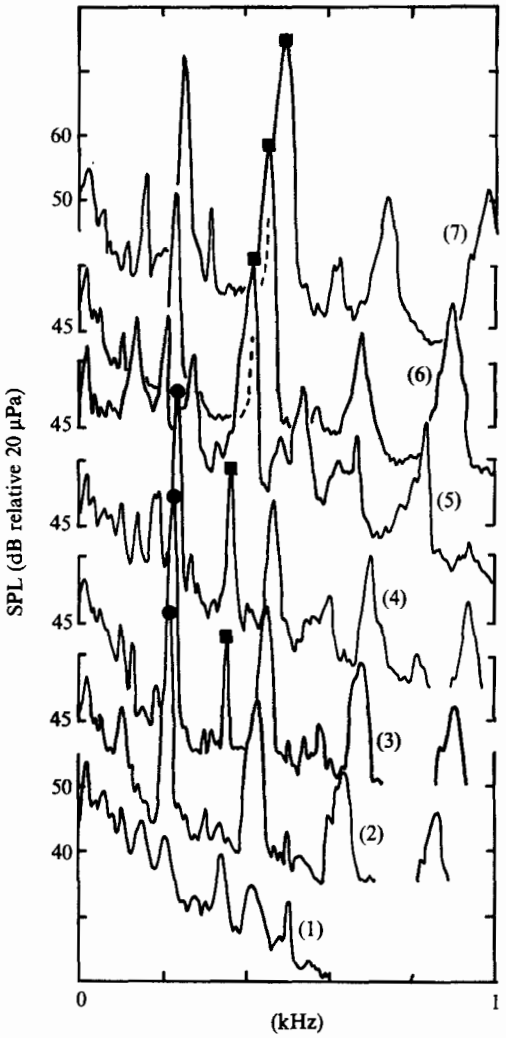

FIGURE 7. Near-field pressure spectra (3.75 Hz bandwidth, averaged over 75 realizations) at $x/D = 0.67$ and $r/D = 1.3$ as a function of density ratio for $Re = 7500$. (1), $S = 0.78$; (2) 0.69; (3), 0.65; (4), 0.62; (5), 0.55; (6), 0.51; (7), 0.47. ●, Mode I; ■, Mode II.

presence of a strong subharmonic at $St \approx 0.45/2$ indicating 'vortex pairing'. In the intermediate range $0.65 \geqslant S \geqslant 0.55$ the jet seems to flip-flop between the two modes and hence both constituents are manifest in the long-time-averaged spectra. When the amplitudes of these two modes, i.e. the height of the marked spectral peaks of figure 7, normalized by the jet dynamic head, are plotted on figure 8 against the density ratio, the similarities to the global behaviour of the cylinder wake, as investigated by Provansal, Mathis & Boyer (1987) and others, become apparent. As in their case, we find that near critical conditions the characteristic overall amplitude $|A|$ of the global response is governed by a Landau equation (Landau & Lifshitz 1959, paragraph 27)

$$\mathrm{d}|A|/\mathrm{d}t = c_1|A| - c_2|A|^3 + \alpha, \tag{1}$$

where a forcing term α has been included for future reference. With the density ratio S as control parameter, the global temporal growth rate c_1 is to leading-order

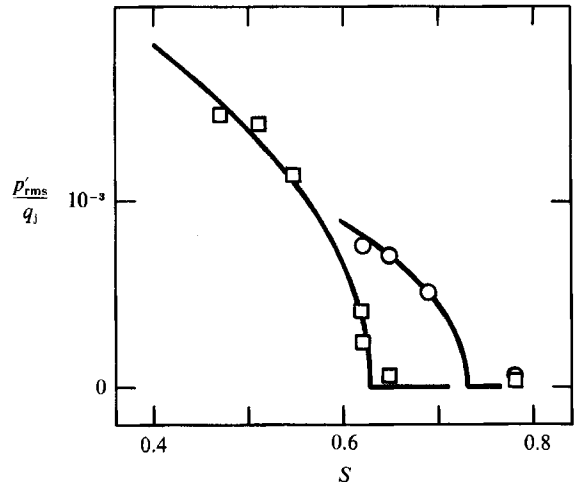

FIGURE 8. Amplitude of the dominant near-field pressure oscillation in figure 7, normalized by the jet dynamic head $q_j = \frac{1}{2}\rho_j U_j^2$, versus density ratio $S = \rho_j/\rho_\infty$. Solid curves are given by equation (2), fitted to the data. ○, Mode I with Strouhal number $St \approx 0.3$ (fitted transition density ratio $S_{crit} = 0.73$); □, Mode II with $St \approx 0.45$ ($S_{crit} = 0.63$).

proportional to $(S_{crit} - S)$. Hence, for zero forcing and a cubic nonlinearity that limits the amplitude, i.e. for $c_2 > 0$, the amplitude $|A|_{sat}$ of the saturated global response is found to depend on S as

$$|A|_{sat} \propto (S_{crit} - S)^{\frac{1}{2}}; \quad \alpha = 0, \quad S \leqslant S_{crit}. \tag{2}$$

This relationship has been fitted to the data of figure 8 for each of the two modes separately and describes the amplitude behaviour well, leading to S_{crit} values of 0.73 and 0.63 respectively. We mention in passing that the normalization of the amplitudes on figure 8 is not essential – the un-normalized data lead to the same S_{crit} values within the uncertainty of approximately ± 0.01. In addition, the amplitude of the first harmonic, at twice the dominant frequency, was found to depend linearly on $(S_{crit} - S)$ for both modes (with a coefficient close to zero for Mode I), as expected from weakly nonlinear theory (Stuart 1971). Despite the fact that not all constants in the Landau equation could be measured as in Provansal *et al.* (1987), this amplitude behaviour strongly supports the existence of supercritical Hopf bifurcations (Joseph 1976, Chapter II) to the two self-excited global modes (limit cycles) at the respective S_{crit} value. When comparing with the locally parallel stability analysis of Monkewitz & Sohn (1986, 1988), we note that the higher S_{crit} of 0.73 ± 0.01 coincides with the absolute instability boundary at $S_{loc} = 0.72$, for which local absolute instability is only found at *one* downstream location. The model analysis of Chomaz *et al.* (1988), on the other hand, suggests that, at S_{crit}, absolute instability should exist over a finite streamwise interval, i.e. that S_{crit} should be strictly smaller than $S_{loc} = 0.72$. At the present time we cannot find a compelling reason for this coincidence – we can only speculate that a weak, long-range feedback (Dimotakis & Brown 1976; Morkovin 1988) may destabilize this first global mode, or that the mean velocity and density profiles for the stability calculations need to be fitted more closely to the experimental data, although a few numerical experiments indicate that the theoretical results are quite insensitive to profile details. Also Sreenivasan *et al.* (1989) report an S_{crit} of 0.6 at a Mach number $M = U_j/a_\infty = 0.15$,

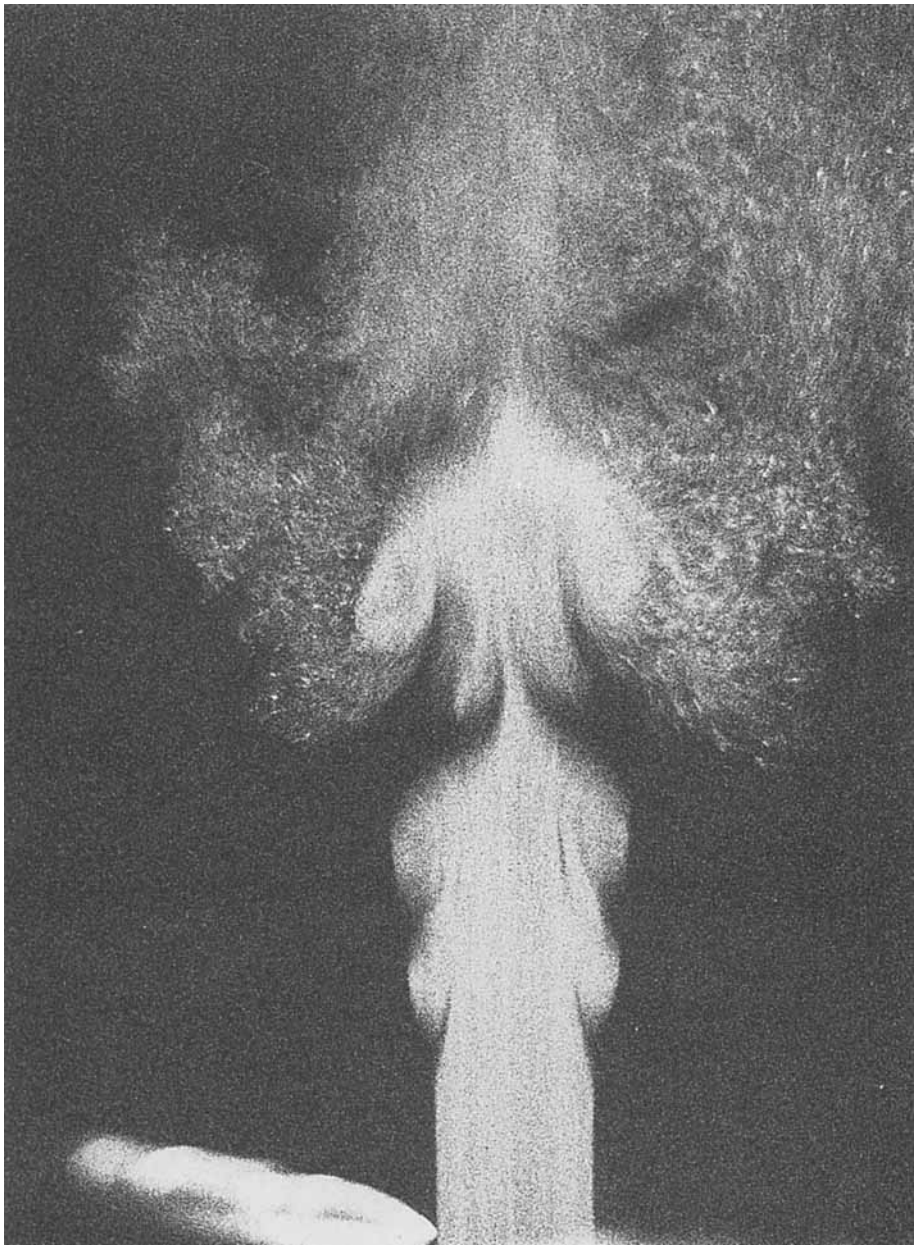

FIGURE 9. Visualization of Mode II at $S = 0.47$ and $Re = 7500$. Smoke illuminated by a laser sheet through the jet axis, strobed at the subharmonic $St = 0.23$ (250 Hz). 1/30 s shutter speed.

which appears to correspond to our second bifurcation. Again, we can only speculate that the discrepancy is due to differences in the experimental set-up.

We now proceed to characterize the two distinctive global modes we observe in our set-up. For a Reynolds number of 7500 and $S = 0.62$ ($T_j = 200$ °C), Mode I dominates (see spectrum (4) of figure 7) and is particularly clearly visualized on figures 2(*b*) and 2(*c*). Consistent with the spectrum, which shows a dominant fundamental and its

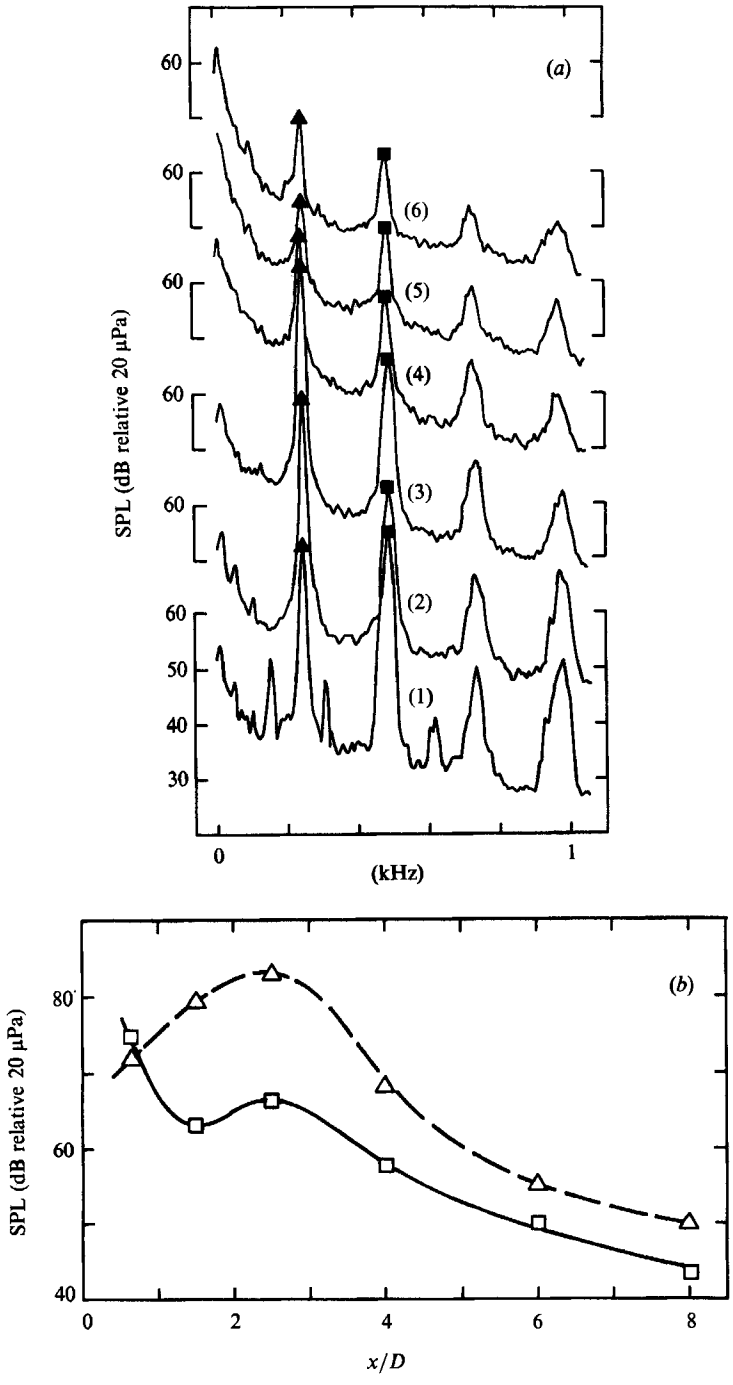

FIGURE 10. Near-field pressure for $S = 0.47$ and $Re = 7500$. (*a*) Spectra (3.75 Hz bandwidth, averaged over 75 realizations) along a ray emanating from $x/D = 0.67$ and $r/D = 1.3$ and inclined 25° with respect to the jet axis: (1), $x/D = 0.67$; (2), 1.5; (3), 2.5; (4), 4; (5), 6; (6), 8. (*b*) Amplitude of subharmonic (△) with $St = 0.225$ and fundamental (□) with $St = 0.45$ versus x/D.

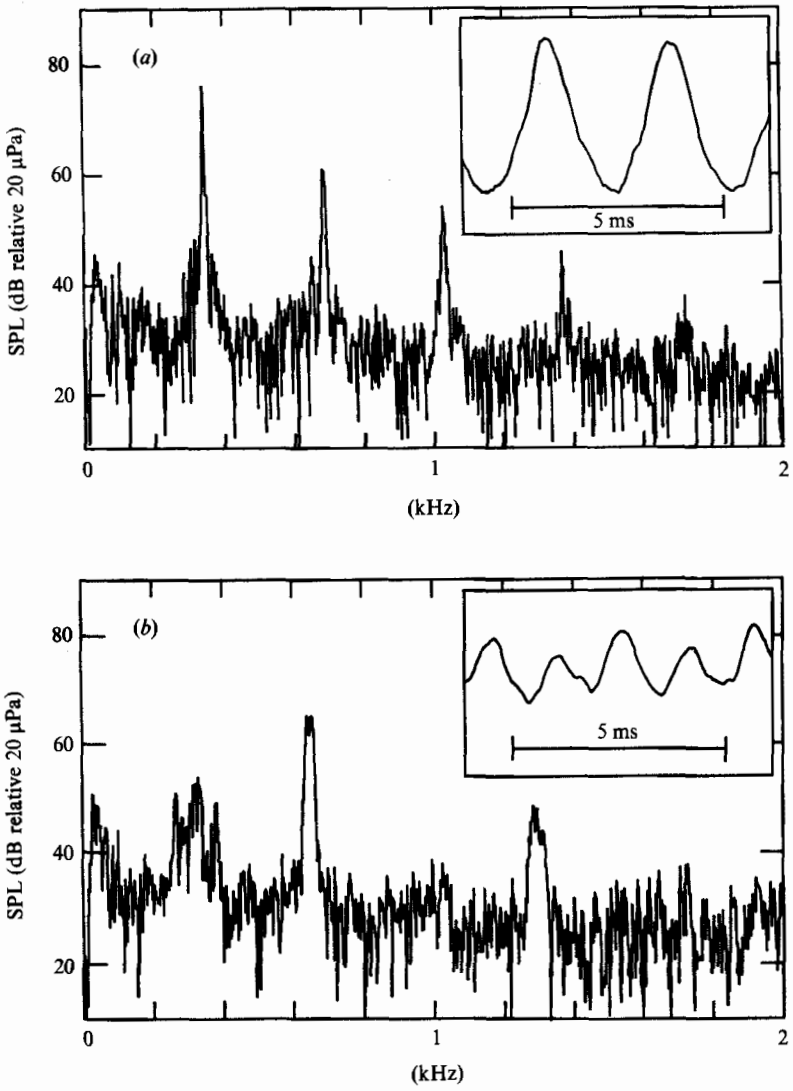

FIGURE 11. Single near-field pressure spectra (3.75 Hz bandwidth) and time traces for $S = 0.47$, $Re = 10^4$, and a nozzle extension of $1D$, showing switching between: (*a*) Mode I with $St = 0.23$; (*b*) Mode II with $St = 0.44$. Inserts show the corresponding time traces.

harmonics, the vortex rings on the schlieren images are equally spaced along the entire jet potential core. Figure 2 (*d*), however, is not so clear and may correspond to one of the brief periods of Mode II oscillations at $Re = 7500$ and $S = 0.62$. The character of this Mode II become much clearer at $Re = 7500$ and $S = 0.47$ (spectrum (7) of figure 7), where Mode I has completely disappeared: as shown on the laser-sheet visualization of figure 9, a distinctive doubling of the vortex-ring spacing occurs around $x/D = 3$. This association of Mode II with 'vortex pairing' is further supported by near-field pressure spectra at different downstream locations, presented on figure 10, which reveals that the subharmonic quickly takes over at about $x/D = 1$ and saturates around $x/D = 3$. The global Mode II is therefore believed

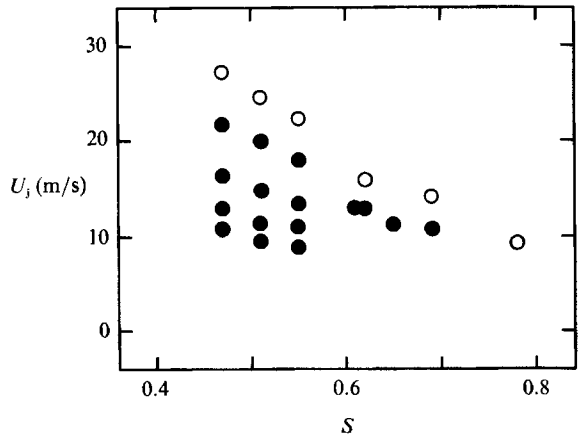

FIGURE 12. Boundary between clearly line-dominated spectra (●) and spectra with broadened lines (○) in the (S, U_j)-plane.

to be a 'compound mode' consisting of a fundamental phase-locked with its subharmonic.

During the course of the experiments we found, as already mentioned, that under certain operating conditions the jet flip-flops between the two modes. Such switching occurs for example with a nozzle extension of $1D$, a density ratio $S = 0.47$ and $Re = 10^4$, where Mode I dominates and Mode II is rather ephemeral, appearing intermittently during approximately 5% of the time. This behaviour is documented on figure 11 where the two distinct modes have been captured by single spectra as well as by the corresponding time traces.

4.2.2. *The effect of Reynolds number*

The next question concerns the boundary of self-excited behaviour as the jet velocity is increased at, say, constant density ratio. Sreenivasan *et al.* (1989) presented their results in the S–Mach number plane (their figure 4), as in this plane they found a boundary quite close to the local absolute instability boundary of Monkewitz & Sohn (1986, 1988). In our set-up we find the transition to be at considerably lower velocities, as evidenced by figure 12, where we use again the dimensional jet velocity to express our ignorance about the true controlling parameter(s). For one density ratio, $S = 0.51$, spectra of near-field pressure, normalized with the jet dynamic head, have already been presented in figure 5 for different jet velocities U_j. For these conditions, the broadening of spectral peaks is seen to occur between a U_j of 20 m/s and 24.7 m/s, almost a factor of three lower than observed by Sreenivasan *et al.* (1989). Moreover, Sreenivasan *et al.* find for their smaller nozzles, but not for their largest 12.7 mm nozzle, a lower velocity limit (e.g. $M = 0.085$ at $S = 0.51$) at which self-excited oscillations vanish, while we observe line spectra down to Mach numbers of approximately 0.025, below which the microphone sensitivity becomes marginal. It is suspected that the thickness of the initial shear layer might be the parameter controlling this lower bound. An indication of this is obtained from our figure 4, where the spectral lines for the longest nozzle extension of $3D$, corresponding to the thickest initial shear layer, are distinctly broader and lower than for the shorter extensions.

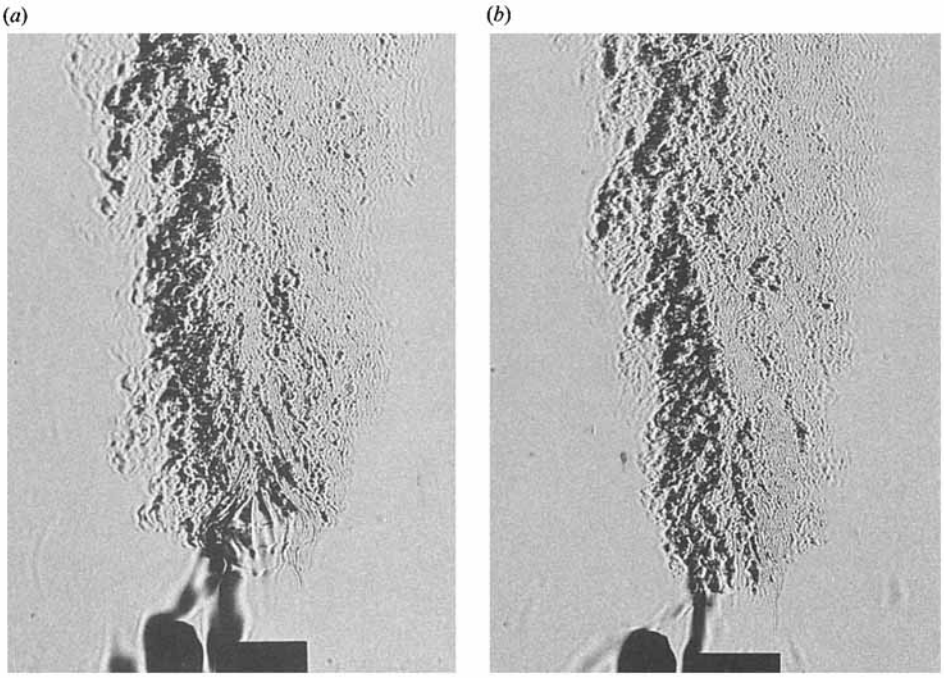

FIGURE 13. Schlieren visualizations of the jet at high velocity, with $S = 0.47$. (*a*) $Re = 2.8 \times 10^4$ ($U_j = 60.7$ m/s), (*b*) $Re = 4.7 \times 10^4$ ($U_j = 103$ m/s).

Furthermore, despite the decrease of the normalized oscillation amplitude towards higher U_j on figure 5, no clear proportionality to $(U_{j,crit} - U_j)^{\frac{1}{2}}$, analogous to the behaviour on figure 8, can be detected. That is, no perfect bifurcation is observed, which suggests that forcing by external (uncontrolled) disturbances becomes important as the velocity is increased at, say, constant density ratio. An argument in support of this suggestion is the increase in the dimensional spatial amplification rate for shear-layer modes (high-frequency modes with wavelengths scaling on the shear-layer thickness and not D) that occurs as the shear layer gets thinner (see for instance Michalke 1984). In other words, the jet becomes an increasingly better amplifier for noise which could conceivably disrupt the phase-lock of a global mode. Visual evidence for the dominance of shear-layer modes at higher velocities is presented on figure 13. The reader is cautioned, however, that the loss of self-excitation at higher Mach/Reynolds number is far from being understood, since, for increasing jet velocities in our facility, the mean temperature profile in the potential core experiences increasingly non-axisymmetric distortions, due to the Péclet number in the steel wool pack of the settling chamber becoming too large (see the considerable distortion at the Reynolds number $Re = 4.7 \times 10^4$ in figure 17).

4.3. *A forcing experiment*

To further support the claim that the observed strong jet oscillations are self-excited, the jet response to acoustic forcing at the natural frequency was investigated. Depending on the stability characteristics of the system, two fundamentally different responses are possible. If the system is convectively unstable everywhere, it is expected to behave as a linear amplifier for sufficiently low forcing amplitudes.

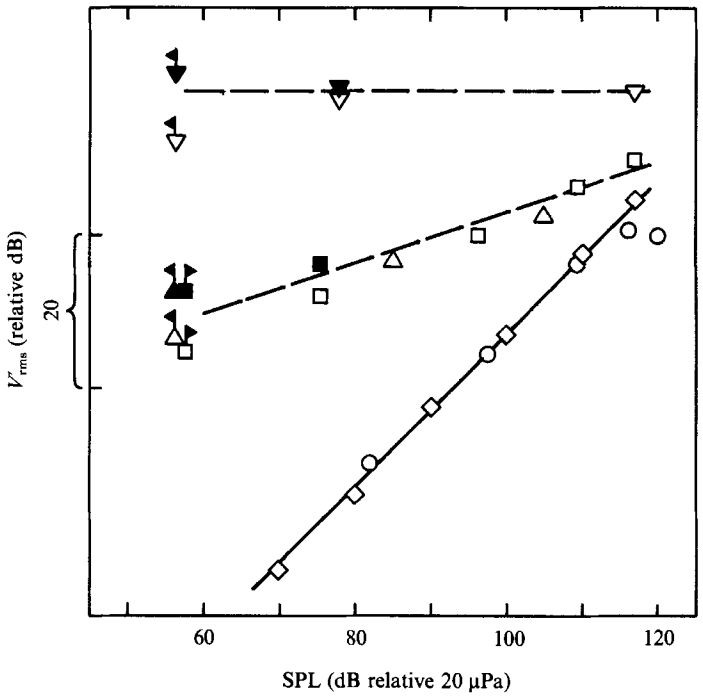

FIGURE 14. Hot-wire output voltage V_{rms} in the jet shear layer at the forcing frequency versus acoustic forcing level. Cold jet with $S = 1$, $U_j = 10$ m/s and hot wire at $x_{HW}/D = 1$ (○); independent repeat (◇); hot jet with $S = 0.49$, $U_j = 12.5$ m/s and $x_{HW}/D = 1$ (□); $S = 0.51$, $U_j = 12.2$ m/s $x_{HW}/D = 1$ (△) and $x_{HW}/D = 2$ (▽). Open and solid symbols represent peak heights of averaged hot-wire spectra (50 realizations) and of single spectra, respectively. Flagged symbols indicate unforced conditions.

On the other hand, if the system is self-excited and sufficiently supercritical, low-amplitude forcing is expected to have little effect on the saturation amplitude. This is easily verified for a system obeying the Landau equation (1), for which

$$|A|_{sat}(\alpha) \approx |A|_{sat}(\alpha = 0) + \alpha/[2|A|^2_{sat}(\alpha = 0)]$$

when $\alpha \ll |A|^3_{sat}(\alpha = 0)$. Around critical conditions, however, the dependence of $|A|_{sat}$ on forcing becomes more pronounced.

For the experiment, a woofer of 35 cm diameter was placed at a lateral distance of 50 cm from the nozzle. A $\frac{1}{4}$ in. B&K microphone at $x/D = 0$ and $r/D = 2$ was used as a reference, while the jet response was monitored by a hot wire at $x/D = 1$ or $x/D = 2$ in the jet shear layer. At each forcing level the radial location of the hot wire was adjusted such as to provide the maximum r.m.s. output which corresponds to an uncalibrated combination of velocity and temperature fluctuations in the heated case. In the latter case it was also verified that the presence of the wire (the probe body being completely outside the jet) did not alter the unforced near-field pressure spectrum. The comparison between the response of the cold jet to forcing at a Strouhal number $St = 0.45$ and the response of the hot jet to forcing at the natural Strouhal number of 0.43 is shown on figure 14. While the cold jet clearly displays the expected linear amplification over two orders of forcing level, no such range is found for the hot jet, which agrees with the findings of Sreenivasan *et al.* (1989) in the helium jet. While some effect of forcing is seen on figure 14 at $x/D = 1$, where the

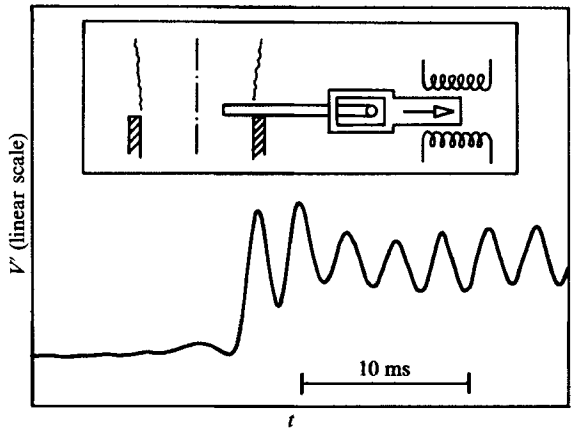

FIGURE 15. Transient of hot-wire output voltage V' in the shear layer at $x/D = 1$ as suppressor (shown to scale on insert) is impulsively retracted from jet with $S = 0.49$ and $U_j = 12.8$ m/s.

amplitude of the global mode is relatively low, the effect at $x/D = 2$ vanishes altogether. Low-frequency variations of the oscillation amplitude are reflected in the difference between data from single and averaged spectra. We note that this x-dependence of the forcing effect cannot be modelled by the Landau equation (1), which is only expected to successfully describe first-order effects, i.e. the effect of forcing on the, say, maximum oscillator amplitude.

4.4. *A transient experiment*

Finally, a transient experiment analogous to the experiments by Provansal *et al.* (1987) in the cylinder wake was attempted. Since neither the jet temperature nor the velocity could be changed rapidly enough to observe the exponential growth phase of self-excited oscillations, other means of suppressing the oscillations had to be found. Inspired by the jet control experiments of Bradbury & Khadem (1975), a pin of 1.5 mm diameter was inserted radially into the jet at $x = 0$, extending 4 mm into the flow. By disturbing the axisymmetry, it effectively suppressed the self-excited oscillations, as monitored by a hot wire in the jet shear layer diametrically opposed to the pin. When the pin was retracted by an electro magnet, the 'oscillator' was found to start up within one period as shown by the time trace of figure 15. Unfortunately, it proved impossible to maintain the jet close enough to critical conditions to allow for the measurement of global temporal growth rates (the coefficient c_1 in (2)). On the other hand, this particular experiment and a similar experiment, carried out independently by Sreenivasan *et al.* (1989), may be of some practical importance. It shows that a very small perturbation of the axisymmetry of the mean flow can suppress the self-excited oscillations and thereby dramatically change the mixing in heated jets and possibly flames (see next section).

5. The jet-spreading in the self-excited regime

The most striking feature of low-density jets undergoing limit-cycle oscillations is the spectacular spreading angle, sometimes with half-angles in excess of 45°, seen on flow visualizations such as figure 2(*b*)–2(*d*). On these figures one also notes that,

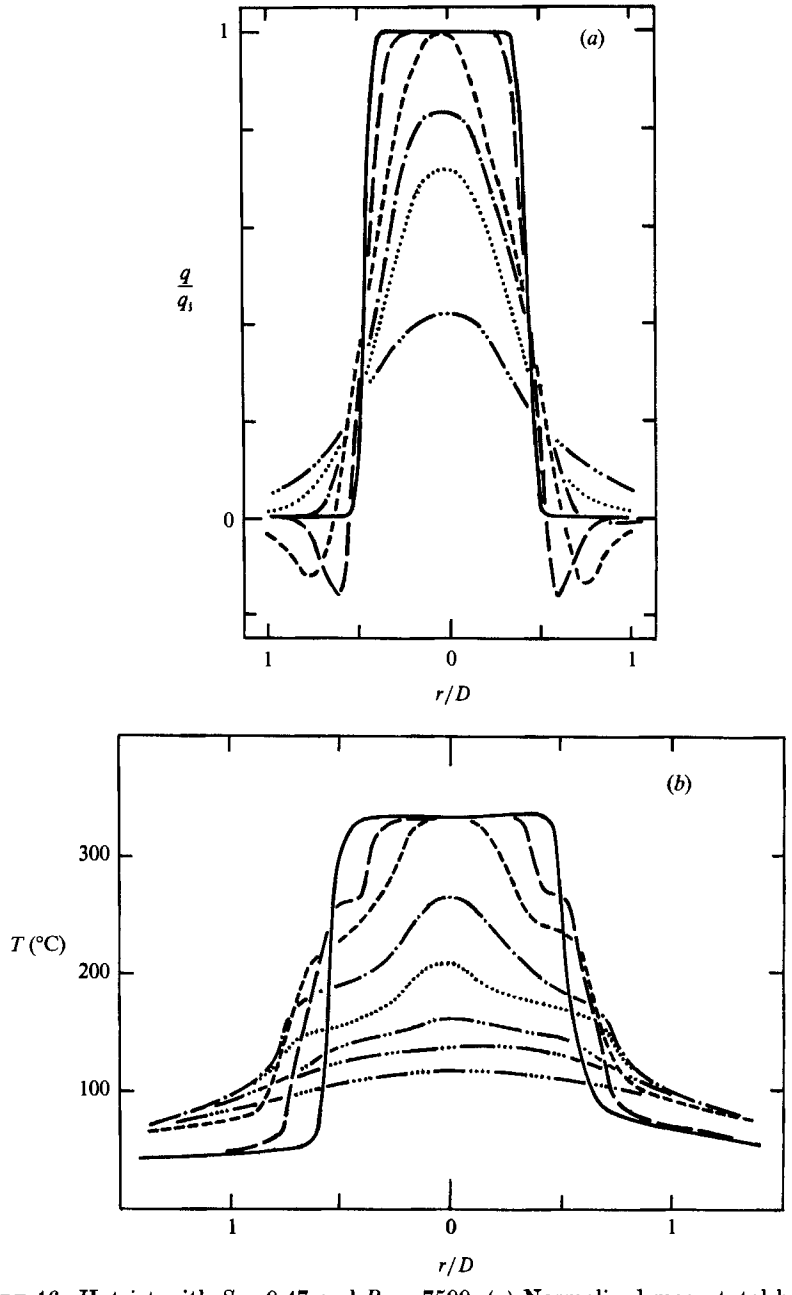

FIGURE 16. Hot jet with $S = 0.47$ and $Re = 7500$. (*a*) Normalized mean total head q/q_j versus r/D at $x/D = 0.67$, 2, 4, 5, 6, 8. (*b*) Mean temperature profiles at $x/D = 0.67$, 2, 3, 4, 5, 6, 8, 10.

under the same conditions, the visual spreading pattern can vary greatly with time. In the following, both the enhanced entrainment, implied by the large spreading, as well as its apparent variability are addressed.

5.1. *Mean flow data*

The first indication of increased entrainment is obtained from the mean total head profiles shown on figure 16(*a*) for a self-excited case with a jet temperature of 350 °C

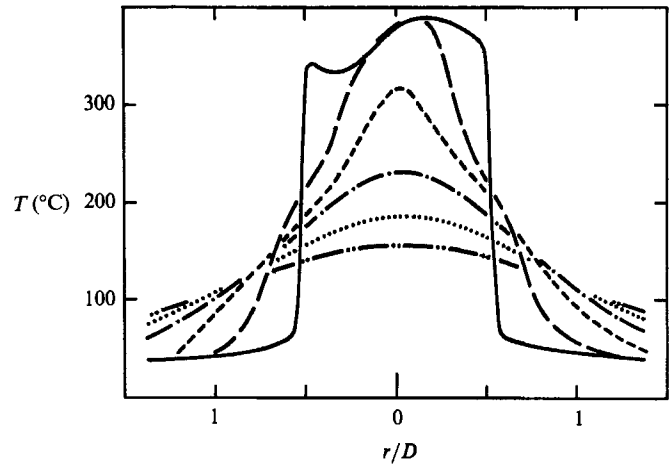

FIGURE 17. Mean temperature profiles versus r/D at $x/D = 0.67, 2, 4, 6, 8, 10$ for $S = 0.47$ and $Re = 4.7 \times 10^4$.

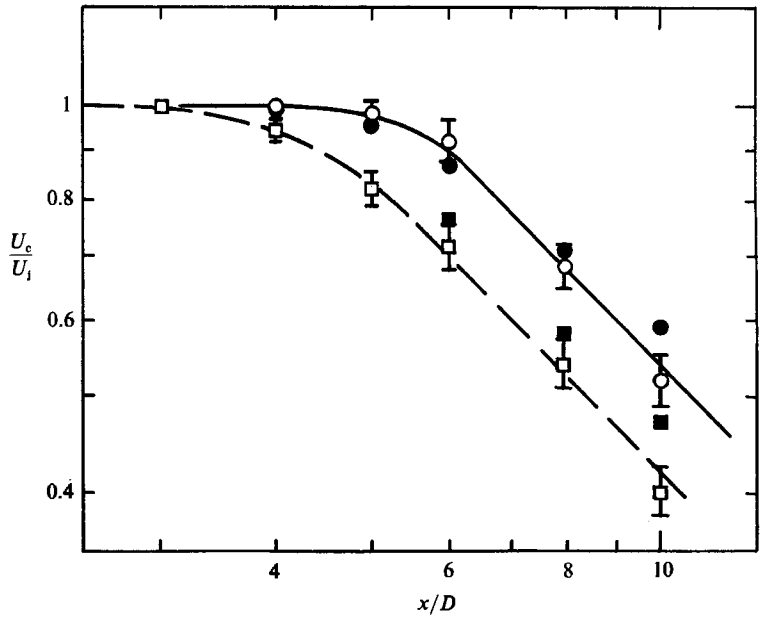

FIGURE 18. Centreline velocity versus x/D for $S = 1$ (○) and $S = 0.47$ (□). Open and solid symbols are for $Re = 7500$ and $Re = 4.7 \times 10^4$, respectively.

and an exit velocity of 16.3 m/s ($Re = 7500$). These data have been collected with a Pitot probe of dimension 0.3×2 mm. The most noteworthy feature of these profiles are the static pressure minima just outside the jet between x/D of approximately 1 and 4.5. The extent of the negative (relative to ambient) pressure region and the value of the minimum – between 10% and 15% of the jet dynamic head q_j – indicate an entrainment that is significantly larger than in the cold case, where negative pressures were only found between x/D of approximately 3 and 4.5 with a minimum of $-0.075q_j$. The corresponding mean temperature profiles are plotted on figure 16(*b*) and, from $x/D = 2$ to about 5, show very clearly intermediate plateaus in the shear

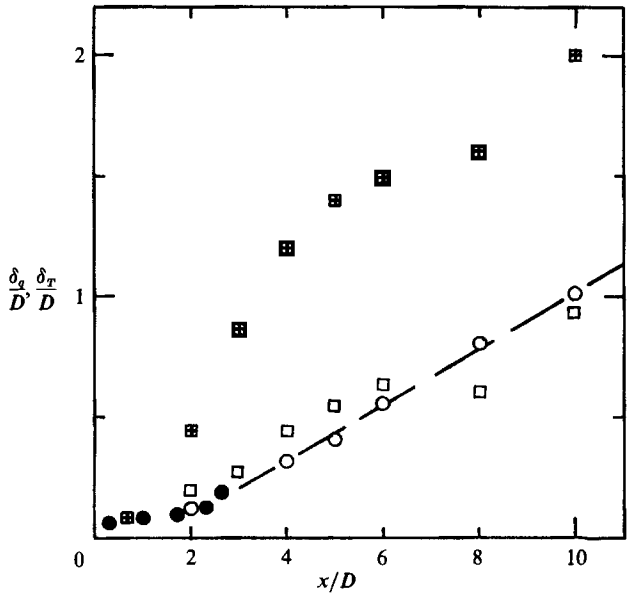

FIGURE 19. Cold jet with $S = 1$: total-head thickness $\delta_q \equiv \Delta q/|\mathrm{d}q/\mathrm{d}r|_{\max}$ for $Re = 10^4$ from Pitot (○) and hot-wire (●) data. Hot jet with $S = 0.47$: total-head thickness δ_q (□) and temperature thickness $\delta_T \equiv \Delta T/|\mathrm{d}T/\mathrm{d}r|_{\max}$ (⊞) for $Re = 7500$.

layers at the radial location of the mixed vortex-ring cores. This confirms the highly organized nature of the primary vortex-ring structures implied by the near-field pressure spectra, and the flow visualization and is in agreement with the findings of Fiedler, Korschelt & Mensing (1978) in a plane mixing layer that was heated on one side and forced acoustically.

To amplify a point made earlier when the effect of Reynolds number was discussed, the loss of temperature axisymmetry at the highest jet Reynolds number $Re = 4.7 \times 10^4$ ($U_j = 103$ m/s) is illustrated by the mean temperature profiles of figure 17 for a density ratio of $S = 0.47$. It is remarkable, though, that despite the severe initial distortion there is still some indication of mixed vortex cores and a complete restoration of axisymmetry by $x/D = 6$. This, and the persistent, distinct peak in the near-field pressure spectra at a constant Strouhal number $St \approx 0.4$ (figure 3 of Monkewitz *et al.* 1988) suggest that, even at this high velocity, a large-scale global mode, probably no longer self-excited, contributes significantly to the jet dynamics. These conclusions are entirely consistent with the decay of the centreline velocity shown on figure 18 which is indicative of the mixing under different conditions: the fastest decay is exhibited by the self-excited, low-velocity jet, closely followed by the hot, high-speed jet while in the cold case the potential core is longest.

Finally, the total-head thickness δ_q and mean temperature thickness δ_T, defined by analogy to the vorticity thickness, are shown on figure 19. It is noted that in the cases where the vortex cores show up as intermediate plateaus on the temperature profile, $|\mathrm{d}T/\mathrm{d}r|_{\max}$ was determined by averaging over the central portion of the temperature jump, i.e. after smoothing out the intermediate plateau. Apart from a modest increase of δ_q owing to heating, the main feature of this figure is the disparity between δ_q and δ_T in the self-excited hot case, which is discussed next.

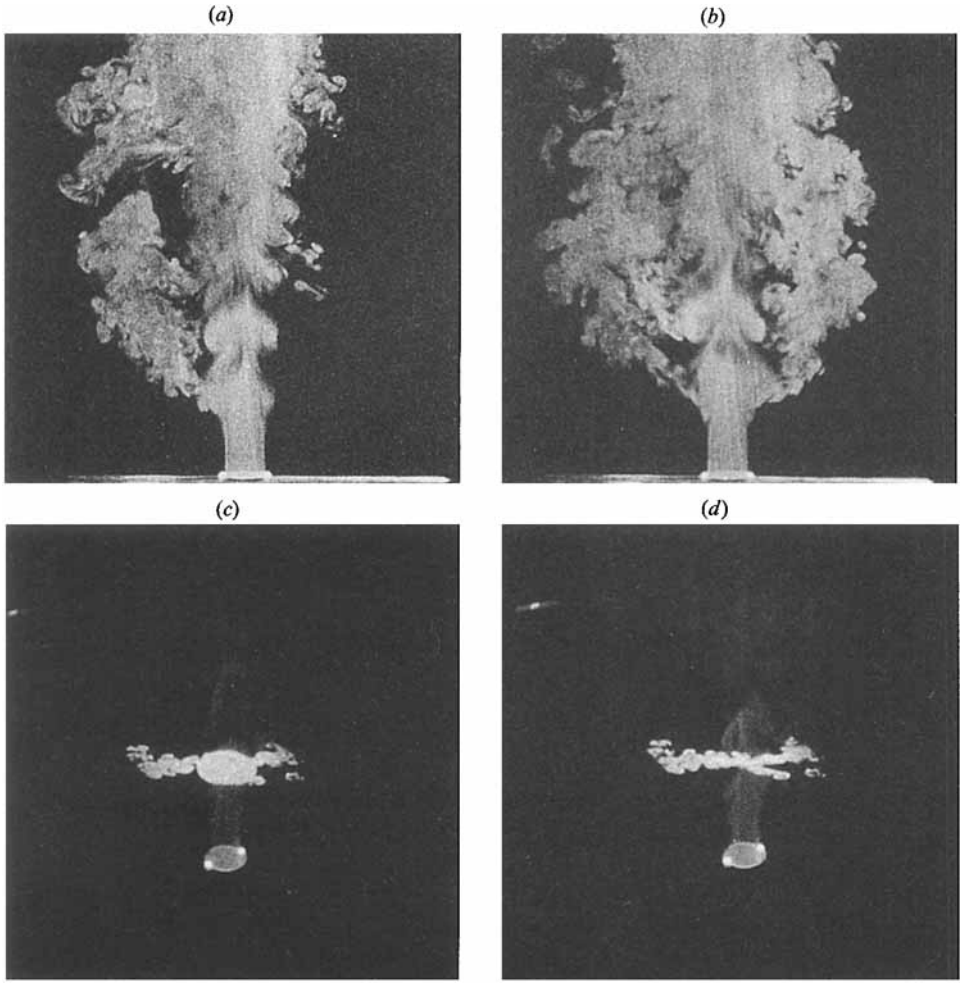

FIGURE 20. Frames from a high-speed movie (500 frames/s ≈ twice the vortex passage frequency) of hot jet at density ratio $S = 0.44$ and $Re = 7500$ with smoke illuminated by laser sheets. (*a*, *b*), Views of longitudinal (x, r)-plane; (*c*, *d*), consecutive frames showing simultaneously longitudinal and cross-sectional (at $x/D = 3$) planes.

5.2. *The visual spreading rate and the generation of 'side jets'*

In a short paper by the present authors (Monkewitz *et al.* 1989, figure 4 in particular) the hypothesis has been put forward that the large jet spreading under self-excited conditions is caused by the Widnall instability (Widnall, Bliss & Tsai 1974) of the primary vortex rings, and the subsequent radial expulsion of 'side-jets' by vortex induction. It has been shown by Monkewitz *et al.* (1989) that these side jets, numbering between 2 and 6, roughly coincide with (x, r)-planes which are approximately equally spaced in the azimuthal direction θ, and move slowly around the jet axis, most likely due to draughts in the laboratory. This motion fully explains the observed variability of the visual spreading pattern in the *side-view*, as the side jets alternately appear and disappear on the image of any *fixed* (x, r)-plane (the laser sheet or focal plane of the Schlieren recording optics).

Although the explanation for the side-jet phenomenon at this point remains

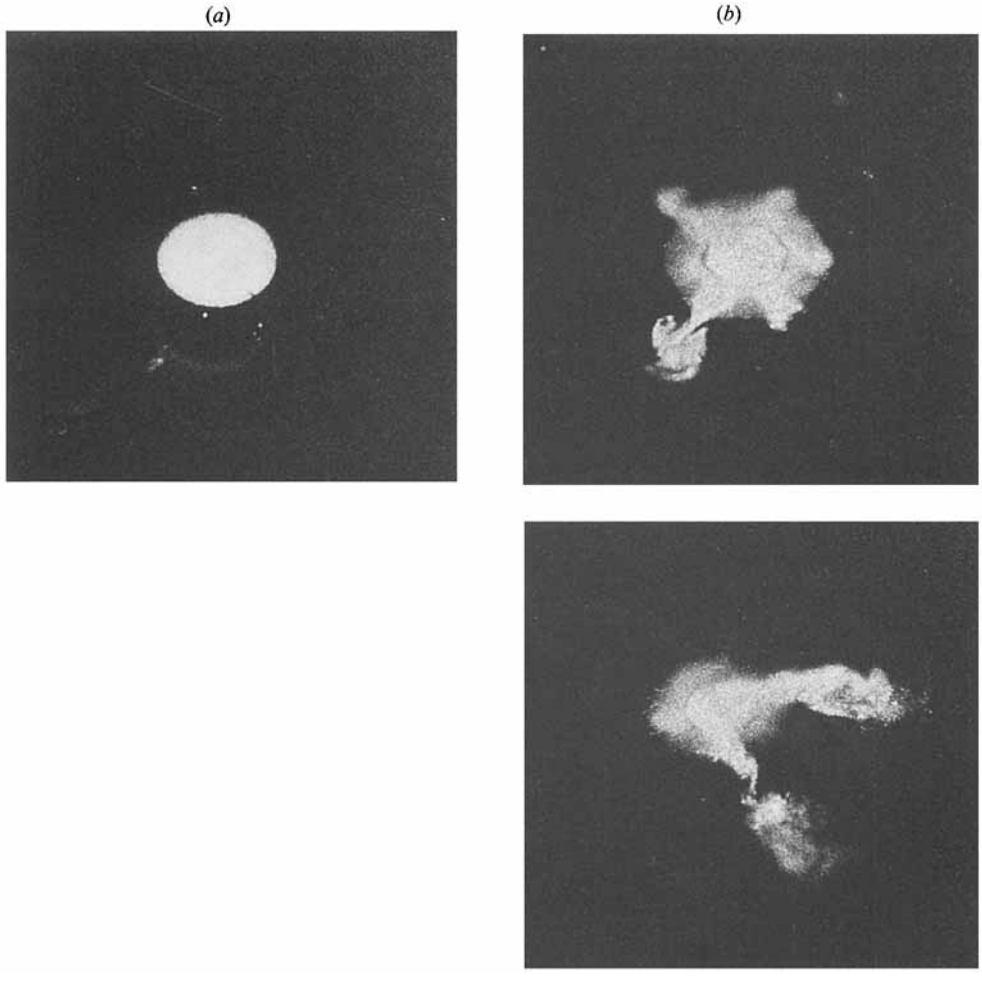

FIGURE 21 (*a*, *b*). For caption see facing page.

tentative and is the subject of further research, additional insight can nevertheless be gained by supplementing the limited flow visualization material presented by Monkewitz *et al.* (1989). First, two frames from a high-speed movie (Barsikow & Lehmann 1988) of the hot jet at 400 °C and $U_j = 17$ m/s are reproduced as figures 20(*a*) and 20(*b*). Notwithstanding their subjective selection, these frames illustrate particularly clearly the general impression from the movie, that the fluid of the side jets is mainly ejected from the core or the immediate neighbourhood of the primary vortex rings. However, the side jets do persist between the ring vortices as demonstrated by two consecutive frames of the same movie, figures 20(*c*) and 20(*d*). They give an oblique view of a (faint) longitudinal section through the seeded jet, illuminated simultaneously with a cross-section at $x/D = 3$. The azimuthal orientation of the longitudinal section is given by the two bright spots near the bottom of the frames, which represent the intersection of the laser sheet with the nozzle rim. Figure 20(*c*) shows a cross-section of a ring vortex as well as two large and one small side jet. Figure 20(*d*), 2 ms later, shows that the side jets indeed persist *between* the primary vortex rings. In fact, a thorough analysis of the movie indicates that the life time of side jets can be as high as hundreds of vortex passage periods.

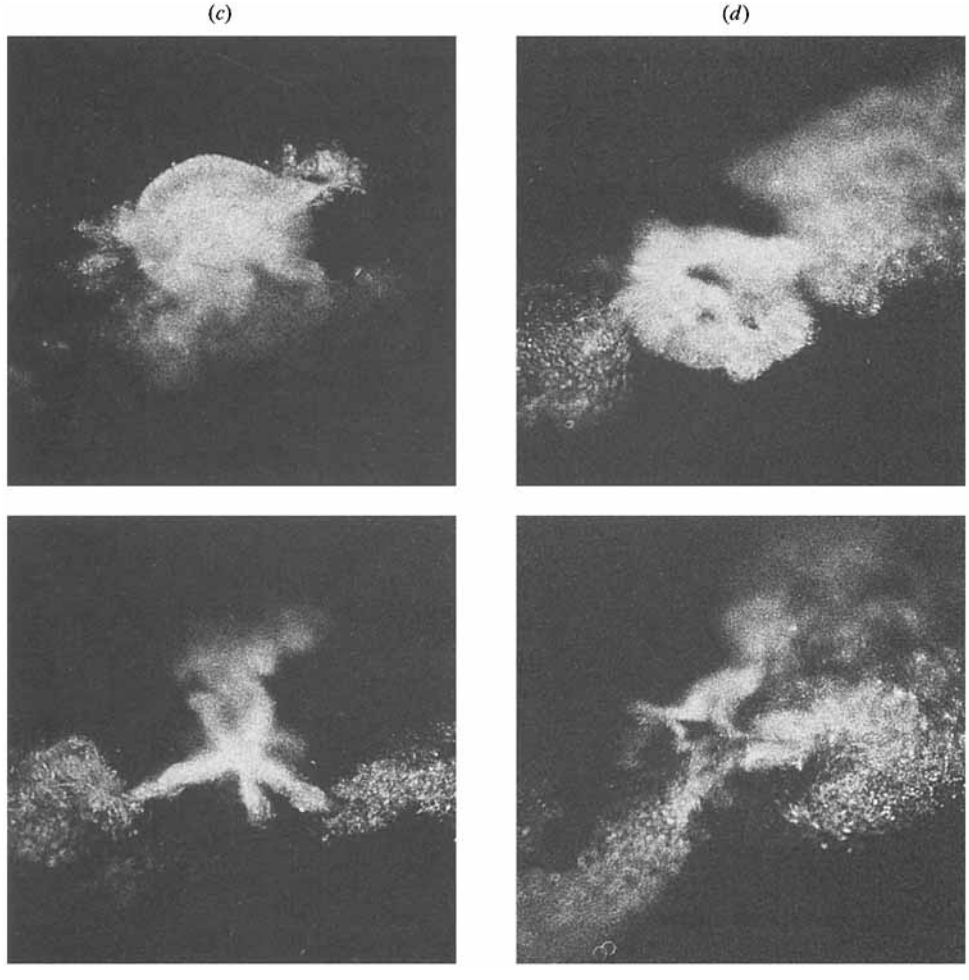

FIGURE 21. Laser cross-sections of the hot jet with $S = 0.45$ and $U_j = 17$ m/s at (*a*) $x/D = 1$, (*b*) $x/D = 2$, (*c*) $x/D = 3$ and (*d*) $x/D = 4$. Stroboscopic illumination at $St = 0.23$. Each reproduction represents four superimposed exposures.

Next, the development of the side jets with downstream distance is illustrated on figure 21 for a self-excited hot jet and on figure 22 for a strongly forced cold jet. The acoustic forcing was effected by placing a 35 cm speaker at a radial distance of 50 cm from the nozzle where it produced a sound pressure level of 94 dB at a Strouhal number of $St \equiv fD/U_j = 0.78$ ($f = 390$ Hz). At each station two stills were selected, one where the laser strobe is synchronized with the passage of a primary vortex ring, and a second that shows the jet cross-section between vortex rings. The first section at $x/D = 1$ has been included to demonstrate the uniform distribution of silicon carbide seeding particles in the jet. Further downstream, the comparison between figures 21 and 22 indicates that there is no qualitative difference between the self-excited and the strongly forced case – the only difference is that, owing to the limited forcing amplitude, the side jets in the cold case form somewhat further downstream. The other minor difference between the self-excited heated jet and the vigorously excited cold jet is the larger number of side jets in the latter. This is easily explained by the higher Strouhal number chosen for the cold jet excitation, because it was

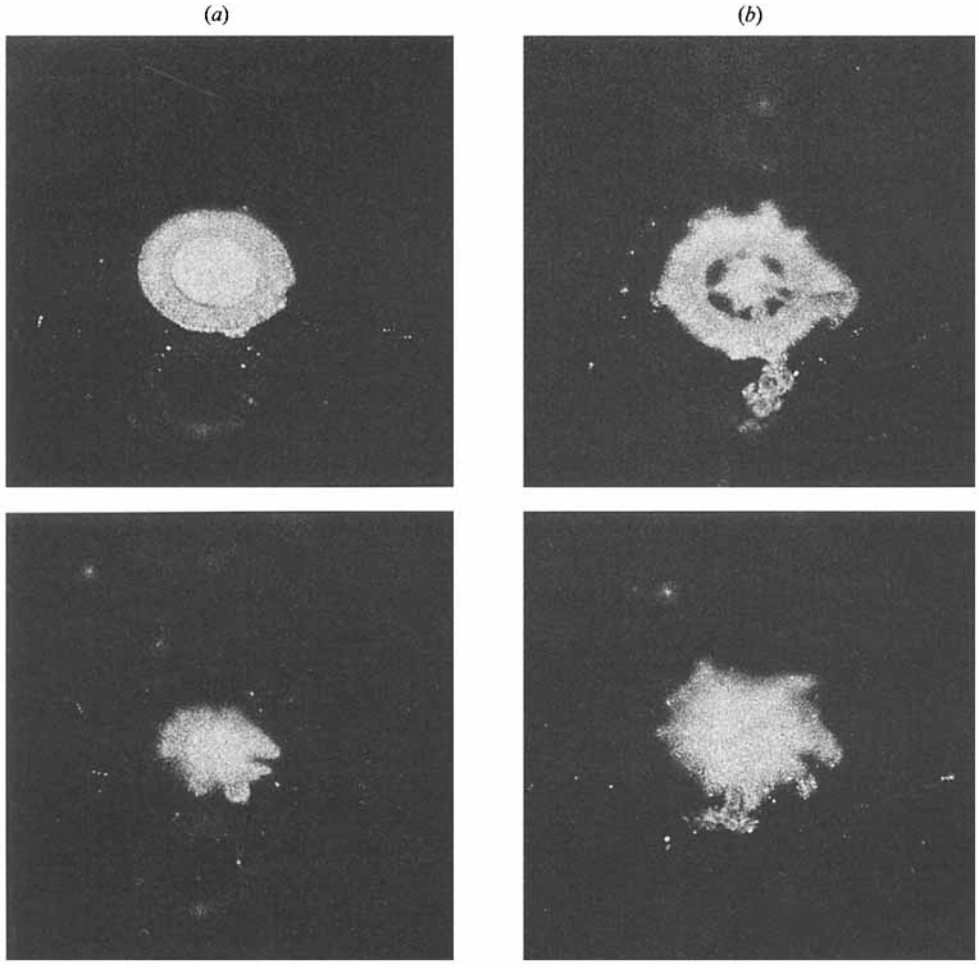

FIGURE 22(a, b). For caption see facing page.

found to yield more stable side jets. The strong similitudes between the two cases therefore support the claim that the formation of substantial side jets depends mainly on the strength and organization of the primary vortex structures and not on the jet density.

We also notice that, between vortex rings and side jets as far upstream as $x/D = 3$, unseeded external air is entrained in a non-axisymmetric fashion almost clear to the jet centre. We therefore re-emphasize the difference between the self- or artificially-excited jet and the unforced homogeneous (cold) jet. In the latter case the formation of axisymmetric large-scale structures and the development of azimuthal structure occurs sequentially, as depicted on Yule's (1978) cartoon, and is analogous to the development of the plane mixing layer studied by Bernal & Roshko (1986) and Lasheras & Choi (1988), for instance. Therefore, the initial entrainment in the non-excited jet is axisymmetric, and corresponds to the situation in the plane mixing layer considered by Dimotakis (1986). Only further downstream does the 'three-dimensionalization' of the primary structures occur, which is associated with a significant generation of smaller scales, variously referred to as small-scale or mixing transition. In contrast, the formation of the primary vortex-ring structures and their

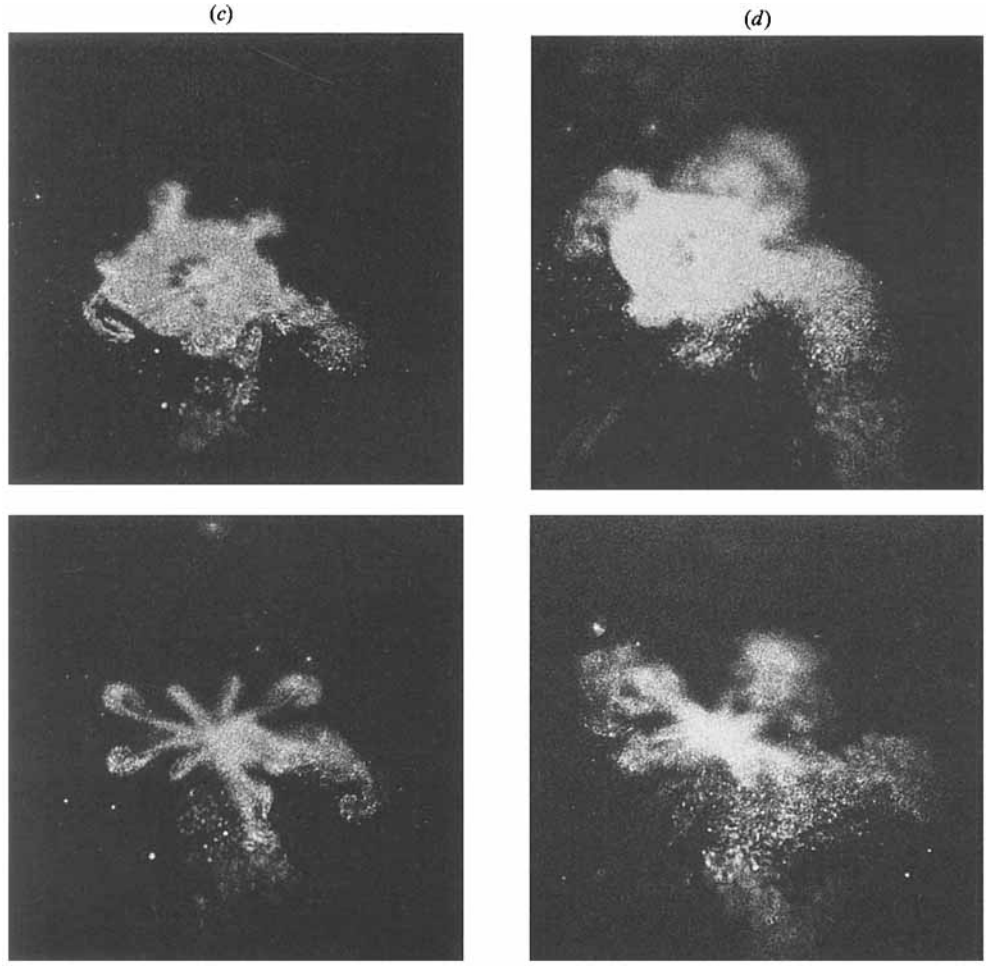

FIGURE 22. Laser cross-sections of the forced cold jet with $U_j = 7.5$ m/s at (*a*) $x/D = 2$, (*b*) $x/D = 3$, (*c*) $x/D = 4$ and (*d*) $x/D = 5$. Forcing at 94 dB sound pressure level (next to the nozzle) and $St = 0.78$. Stroboscopic illumination at the subharmonic $St = 0.39$. Each reproduction represents between three and six superimposed exposures.

'three-dimensionalization' appear to occur *simultaneously* in the strongly excited jet, leading immediately to non-axisymmetric entrainment and the production of smaller scales associated with mixing.

6. Conclusions

A transitional, heated, axisymmetric air jet has been shown to develop self-excited oscillations below a density ratio of approximately 0.73 that corresponds to the formation of a regular sequence of intense vortex ring structures. It has been demonstrated that the local stability characteristics of the jet, i.e. absolute or convective instability, provide a useful guide to the global behaviour, in this case correctly indicating the presence of bifurcations to time-amplified global modes.

While the questions relating to the primary large-scale structures have been resolved quite satisfactorily with stability theory as a guide, the interaction between these large structures and shear-layer modes of small wavelength, scaling on the jet

shear-layer thickness and highly amplified at large Reynolds numbers, remains to be clarified. What we have shown is that the small scales appear to be able to introduce enough jitter into the primary structures to disrupt their perfect phase-lock. Besides that, the existence of turbulence in the shear layer also leads to more stable mean velocity profiles which tend to inhibit self-excitation.

The at times spectacular spreading of self-excited hot jets has been linked to the formation of side jets. The exploration of their geometry and motion has permitted a full explanation of the observed variability of the visual jet spreading. In this connection we have also found that the first, large-scale induction phase of entrainment in a self-excited jet is strongly non-axisymmetric with an associated increase of mixing. Regarding the generation mechanism for the vigorous side jets, the hypothesis that they are the result of induction by the wavy primary vortex rings still awaits confirmation. What has been established by comparison with strongly forced cold jets, however, is that the strength of the primary vortex rings is the key parameter governing their formation.

The financial support of this project by TECFLAM as well as the stimulating discussions with Professor A. Michalke and Dr E. Pfizenmaier are gratefully acknowledged. One of us (P.A.M.) also wishes to thank the DLR and the Hermann-Foettinger Institut for their kind hospitality and support during his stay in Berlin and the Air Force Office of Scientific Research for its support under Grant 87-0329 after his return to the US.

REFERENCES

BARSIKOW, B. & LEHMANN, B. 1988 Orderly structures in a heated circular jet. Award winning video at the "Gallery of Fluid Motion", 41st Ann. Meeting of the Div. of Fluid Dynamics, Am. Phys. Soc., Buffalo N.Y. Some frames reproduced in Reed, H. L. 1989 Gallery of fluid motion. *Phys. Fluids* A **1**, 1445.

BERNAL, L. P. & ROSHKO, A. 1986 Streamwise vortex structure in plane mixing layers. *J. Fluid Mech.* **170**, 499.

BERS, A. 1983 *Basic Plasma Physics I* (ed. A. A. Galeev & R. N. Sudan), p. 451. North-Holland.

BRADBURY, L. J. S. & KHADEM, A. H. 1975 The distortion of a jet by tabs. *J. Fluid Mech.* **70**, 801.

CHOMAZ, J. M., HUERRE, P. & REDEKOPP, L. G. 1988 Bifurcations to local and global modes in spatially developing flows. *Phys. Rev. Lett.* **60**, 25.

CORRSIN, S. & UBEROI, M. S. 1947 Experiments on the flow and heat transfer in a heated turbulent air jet. *NACA TN* 1865.

DIMOTAKIS, P. E. 1986 Two-dimensional shear-layer entrainment. *AIAA J.* **24**, 1791.

DIMOTAKIS, P. E. & BROWN, G. L. 1976 The mixing layer at high Reynolds number: large-structure dynamics and entrainment. *J. Fluid Mech.* **78**, 535.

FIEDLER, H., KORSCHELT, D. & MENSING, P. 1978 On transport mechanism and structure of scalar field in a heated plane shear layer. In *Structure and Mechanisms of Turbulence II* (ed. H. Fiedler). Lectures Notes in Physics, Vol. 76, p. 58. Springer.

FUCHS, V., KO, K. & BERS, A. 1981 Theory of mode-conversion in weakly inhomogeneous plasma. *Phys. Fluids* **24**, 1251.

HUERRE, P. & MONKEWITZ, P. A. 1985 Absolute and convective instabilities in free shear layers. *J. Fluid Mech.* **159**, 151.

HUERRE, P. & MONKEWITZ, P. A. 1990 Local and global instabilities in spatially developing flows. *Ann. Rev. Fluid Mech.* **22**, 473.

HUSSAIN, A. K. M. F. & HASAN, M. A. Z. 1983 The 'whistler-nozzle' phenomenon. *J. Fluid Mech.* **134**, 431.

HUSSAIN, A. K. M. F. & ZAMAN, K. B. M. Q. 1978 The free shear layer tone phenomenon and probe interference. *J. Fluid Mech.* **87**, 349.

JOSEPH, D. D. 1976 *Stability of Fluid Motions I.* Springer.

KYLE, D. 1988 LIF images of He/N_2 jets. *Mech. Engng Rep.* FM88DK1. Yale University.

LANDAU, L. D. & LIFSHITZ, E. M. 1959 *Fluid Mechanics.* Pergamon.

LASHERAS, J. C. & CHOI, H. 1988 Three-dimensional instability of a plane shear layer: an experimental study of the formation and evolution of streamwise vortices. *J. Fluid Mech.* **189**, 53.

LEHMANN, B., BARSIKOW, B., MONKEWITZ, P. A., BECHERT, D. W. & EICKHOFF, H. 1988 Experimentelle Analyse der Instabilitätsformen in Heissgas-Freistrahlen und Freistrahlflammen (Experimental analysis of the instability modes of hot gas jets and jet flames). *Proc. 4th TECFLAM Seminar on Turbulent Combustion, Stuttgart, November 3.*

LEPICOVSKI, J., AHUJA, K. K., BROWN, W. H., SALIKUDDIN, M. & MORRIS, P. J. 1988 Acoustically excited heated jets. *NASA CR* 4129, part I-III.

MICHALKE, A. 1971 Instabilität eines kompressiblen runden Freistrahls unter Berücksichtigung des Einflusses der Strahlgrenzschichtdicke. *Z. Flugwiss.* **19**, 319.

MICHALKE, A. 1984 Survey on jet instability theory. *Prog. Aerospace Sci.* **21**, 159.

MONKEWITZ, P. A. 1988 The absolute and convective nature of instability in two-dimensional wakes at low Reynolds numbers. *Phys. Fluids* **31**, 999.

MONKEWITZ, P. A. & BECHERT, D. W. 1988 Gallery of fluid motion. *Phys. Fluids* **31**, 2386.

MONKEWITZ, P. A., BECHERT, D. W., BARSIKOW, B. & LEHMANN, B. 1988 Experiments on the absolute instability of heated jets. In *Advances in Turbulence* II (ed. H.-H. FERNHOLZ & H. E. FIEDLER), p. 455. Springer.

MONKEWITZ, P. A., HUERRE, P. & CHOMAZ, J. M. 1987 Preferred modes in jets and global instabilities. *Bull. Am. Phys. Soc.* **32**, 2051.

MONKEWITZ, P. A., LEHMANN, B., BARSIKOW, B. & BECHERT, D. W. 1989 The spreading of self-excited hot jets by side-jets. *Phys. Fluids* A **1**, 446.

MONKEWITZ, P. A. & SOHN, K. D. 1986 Absolute instability in hot jets and their control. *AIAA Paper* 86-1882.

MONKEWITZ, P. A. & SOHN, K. D. 1988 Absolute instability in hot jets. *AIAA J.* **26**, 911.

MORKOVIN, M. V. 1988 Recent insights into instability and transition to turbulence in open flow systems. *AIAA paper* 88-3675.

PROVANSAL, M., MATHIS, C. & BOYER, L. 1987 Bénard–von Kármán instability: transient and forced regimes. *J. Fluid Mech.* **182**, 1.

SREENIVASAN, K. R., RAGHU, S. & KYLE, D. 1989 Absolute instability in variable density round jets. *Exps. Fluids* **7**, 309.

STUART, J. T. 1971 Nonlinear stability theory. *Ann. Rev. Fluid Mech.* **3**, 347.

SUBBARAO, E. R. 1987 An experimental investigation of the effects of Reynolds number and Richardson number on the structure of a co-flowing buoyant jet. Ph.D. thesis, Stanford University.

TYNDALL, J. 1867 *Sound – A Course of Eight Lectures Delivered at the Royal Institution of Great Britain.* London: Longmans, Green and Co.

WIDNALL, S. E., BLISS, D. B. & TSAI, C.-Y. 1974 The instability of short waves on a vortex ring. *J. Fluid Mech.* **66**, 35.

YULE, A. J. 1978 Large-scale structure in the mixing layer of a round jet. *J. Fluid Mech.* **89**, 413.